Second-order work analysis for granular materials using a multiscale approach

François Nicot, Nejib Hadda, F. Darve

Second-order work analysis for granular materials using a multiscale approach

François Nicot[1,*,†], Nejib Hadda[1] and Félix Darve[2]

[1]CEMAGREF, Grenoble, France
[2]UJF-INPG-CNRS, Laboratoire Sols Solides Structures Risques, Grenoble, France

It has been established that the second-order work criterion is a general necessary condition for all instabilities by divergence in rate-independent granular materials. The relation between the values of discrete second-order work at the intergranular contact point level and its global macroscopic value is recalled at the beginning of this paper. Then, the basic purpose of the paper is tackled by an analysis of the main features of second-order work criterion in relation with the granular microstructure. For that, it is considered a novel micromechanical model (the so-called '*H*-microdirectional model'), which has the property to involve three scales: grain scale, mesoscale with a specific granular configuration and continuum mechanics macroscale. Eventually, these exhibited features (a bifurcation stress domain and some instability cones) are qualitatively compared with the ones provided by direct numerical simulations issued from a discrete element model. The ultimate goal is to analyse what happens at the granular scale, when the macrosecond-order work is vanishing at the macrolevel.

Keywords: stress; large deformations; second-order work; granular materials; homogenization; multiscale; micromechanics; microstructure; failure; instability

1. INTRODUCTION

The second-order work criterion (see e.g. [1–3]) is increasingly being applied to analyse failures in geomaterials. Indeed, it has been shown recently [4, 5] that this is the correct criterion to detect any divergence instability in rate-independent non-associate materials. It may be recalled that instabilities can be classified into two main classes: divergence instabilities lead to failure by suddenly and monotonously increasing strains, whereas flutter instabilities are defined by cyclically increasing strains until total failure. Considering now only divergence instabilities, the bifurcation/failure stress domain delimited by the vanishing values of the determinant of the elasto-plastic stiffness matrix on the one hand and the determinant of the symmetric part of this matrix on the other hand contains all the possible failure states (with localized or diffuse modes). Moreover, the second-order work condition contains all the other failure criteria as particular cases [4, 5]. In mathematical terms, the second-order work criterion can be introduced through an 'optimization' scheme. Indeed, the first failure mode possibly reached for the lowest loading level corresponds to the first vanishing of second-order work in a given loading direction, related to the first vanishing of the determinant of the symmetric part of the constitutive matrix.

The main purpose of this paper is to consider this criterion from micromechanical points of view, provided first by a micromechanical constitutive model (the *H*-microdirectional model; [6]) and then by a discrete element method ('YADE' code; [7]).

*Correspondence to: François Nicot, CEMAGREF, Grenoble, France.
†E-mail: francois.nicot@cemagref.fr

In the first part of the paper, the Eulerian and Lagrangian macroscopic and microscopic expressions of second-order work are recalled. It should be stressed that the microscopic expression is the sum of the discrete second-order works at intergranular contacts plus unbalanced terms in dynamic conditions, corresponding to known phenomena called 'local granular avalanches'. Then, the purpose of the second part is to present briefly the micromechanical model, which will be used at a later stage to investigate the second-order work criterion from a microscopic viewpoint. The '*H*-microdirectional model' is characterized by the introduction of three scales: microscale, mesoscale and macroscale. The rather novel intermediate scale essentially enables the kinematics description of the granular medium to be enriched. Two tensorial zones are identified, one roughly 'elastic' and the other roughly 'plastic'.[‡] It will be shown that the second-order work takes negative values inside the plastic tensorial zone (this is a theoretical constraint; the second-order work is a definite, positive quadratic form in the elastic tensorial zone; [8]), just close to its border, according to this micromechanical constitutive model.

On the other hand, it is well established today that direct numerical simulations by a discrete element method (DEM) can give very realistic simulations of the mechanical behaviour of granular media (see e.g. [9]). Thus, it is valuable to check with a discrete element method both the analytical results linking macroscopic and microscopic expressions of second-order work (obtained in the first part of the paper) and the numerical results given by the micromechanical constitutive model (presented in the second part). The observed slight differences between these three approaches (analytical, micromechanical and numerical) are discussed in detail.

All (first-order or second-order) tensorial quantities will be noted with a (simple or double) overbar. According to the usual soil mechanics convention, both strain and stress are positive in compression.

2. LAGRANGIAN AND EULERIAN FORMULATIONS OF SECOND-ORDER WORK

2.1. Macroscopic tensorial formulation

Consider a material body of volume V_0 enclosed by a boundary (Γ_0) in an initial configuration C_0 so as to describe its motion under external loading in an incremental formulation. Following a certain loading history, the body is in a strained configuration C and occupies a volume V of boundary (Γ), in equilibrium under a prescribed external loading. This loading is controlled by specific static or kinematic parameters, referred to as loading parameters.

Let the transformation χ associating each material point $\bar{x}$ of the current configuration C with a corresponding material point $\bar{X}$ of the initial configuration C_0 be introduced such that $\bar{x} = \chi(\bar{X})$. Any field $f(\bar{x})$ of the current positions $\bar{x}$ can be transformed into a field $\widetilde{f}(\bar{X}) = f(\bar{x})$ of the initial positions $\bar{X}$. When no confusion is possible, the notation '~' will be omitted. Because the map χ is bijective, the Jacobian J of the tangent linear transformation $\bar{\bar{F}}$ is strictly positive, with the latter being a function of the positions $\bar{X}$ and $\widetilde{F}_{ij} \partial x_i / \partial X_j$. The displacement field $\bar{u}(\bar{x})$ of material points $\bar{x}$ between both initial and current configurations is defined by the relation $\bar{x} = \chi(\bar{X}) = \bar{X} + \bar{u}(\bar{x}) = \bar{X} + \widetilde{\bar{u}}(\bar{X})$.

The current configuration C at time t is considered to be an equilibrium state. The second-order time differentiation of the kinetic energy written in Lagrangian description [2, 8] is

$$\delta^2 E_c(t) = W_2^{\text{ext}} - W_2^{\text{int}} \tag{1}$$

where $W_2^{\text{ext}} = \int_{\Gamma_0} \delta f_i \ \delta\widetilde{u}_i \ dS_0$ is the external second-order work, involving the loading parameters (surface forces and displacements) acting on the boundary (Γ_0) of the body, and $W_2^{\text{int}} = \int_{V_0} \delta\Pi_{ij} \ \dfrac{\partial(\delta\widetilde{u}_i)}{\partial X_j} \ dV_0$ is the conventional (internal) second-order work following a semi-Lagrangian formalism [10]. $\bar{\bar{\Pi}}$ is the first

[‡]The elastic tensorial zone encompasses all the stress (or strain) incremental directions along which the material behaves elastically. The plastic tensorial zone encompasses all the stress (or strain) incremental directions along which the material behaves plastically.

Piola–Kirchoff stress tensor and $\bar{f}$ the current surface forces applied to the initial (reference) configuration. In what follows, as used in the literature, the internal second-order work will be denoted W_2, and the term 'internal' will be omitted.

The equation $\delta^2 E_c(t) = W_2^{\text{ext}} - W_2^{\text{int}}$ means that, when the internal second-order work takes a zero value according to the material's behaviour, then the sign of $\delta^2 E_c(t)$ corresponds to the sign of the external second-order work. Thus, if the loading applied to the system is associated with a strictly positive value of the external second-order work, then the term $\delta^2 E_c(t)$ becomes strictly positive. Starting from an equilibrium configuration, the kinetic energy increases (outburst of kinetic energy), which was thought to be a mark of instability [6]. The prevalent static equilibrium is no longer possible, and a bifurcation towards a dynamic regime suddenly emerges. For this reason, the characterization of loadings leading to negative values of the second-order work will be thoroughly investigated in the manuscript.

The second-order work formulated in Eulerian description involves the Cauchy stress tensor $\bar{\bar{\sigma}}$. By using the change in variables $\bar{x} = \chi(\bar{X})$, both $\bar{\bar{\sigma}}$ and $\bar{\bar{\Pi}}$ stress tensors are related through the Piola relation, that is,

$$\bar{\bar{\Pi}} = J \; \bar{\bar{\sigma}} \; \left(\bar{\bar{F}}^{-1}\right)^t \tag{2}$$

After differentiation and rearranging terms, Eq. (2) gives

$$\bar{\bar{\delta}} = J\,\delta\bar{\bar{\sigma}} \left(\bar{\bar{F}}^{-1}\right)^t + \delta J\,\bar{\bar{\sigma}} \left(\bar{\bar{F}}^{-1}\right)^t - J\,\bar{\bar{\sigma}} \left(\bar{\bar{F}}^{-1}\right) \left(\delta\bar{\bar{F}}\right)^t \left(\bar{\bar{F}}^{-1}\right)^t \tag{3}$$

or equivalently,

$$\delta\bar{\bar{\sigma}} = \frac{1}{J}\,\delta\bar{\bar{\Pi}} \left(\bar{\bar{F}}\right)^t - \frac{\delta J}{J}\,\bar{\bar{\sigma}} + \frac{1}{J}\,\bar{\bar{\Pi}} \left(\delta\bar{\bar{F}}\right)^t \tag{4}$$

When the two configurations C_0 and C coincide at time t (as in an updated Lagrangian description), $\bar{\bar{\Pi}} = \bar{\bar{\sigma}}$, $\bar{\bar{F}} = \bar{\bar{I}}$ and $J = 1$. However, as the current configuration C will evolve from time t, $\delta\bar{\bar{F}} \neq 0$, and $\delta J \neq 0$. Owing to the updating of configurations, Eqs (3) and (4) simplify into

$$\delta\bar{\bar{\Pi}} = \delta\bar{\bar{\sigma}} + \frac{\delta J}{J}\,\bar{\bar{\sigma}} - \bar{\bar{\sigma}} \left(\delta\bar{\bar{F}}\right)^t = \delta\bar{\bar{\sigma}} + \frac{\delta J}{J}\,\bar{\bar{\Pi}} - \bar{\bar{\Pi}} \left(\delta\bar{\bar{F}}\right)^t \tag{5}$$

and

$$\delta\bar{\bar{\sigma}} = \delta\bar{\bar{\Pi}} - \frac{\delta J}{J}\,\bar{\bar{\Pi}} + \bar{\bar{\Pi}} \left(\delta\bar{\bar{F}}\right)^t \tag{6}$$

As expected in a Eulerian formulation where the boundaries of the material body change continuously, the incremental Cauchy stress tensor in Eq. (6) is composed of three terms:

- $\bar{\bar{\delta}}$ accounting for the change in forces acting in a fixed configuration,
- $-(\delta J/J)\bar{\bar{}}$ accounting for the change in the bulk volume and
- $\bar{\bar{}}\left(\delta\bar{\bar{F}}\right)$ related to the change in the geometrical configuration under constant forces.

By virtue of Eq. (3), the second-order work can be expressed in a Eulerian formulation:

$$W_2 = \int_{v_0} J \left(\delta\bar{\bar{\sigma}} + \frac{\delta J}{J}\,\bar{\bar{\sigma}} - \bar{\bar{\sigma}} \left(\bar{\bar{F}}^{-1}\right)^t\right) \left(\bar{\bar{F}}^{-1}\right)^t : \delta\bar{\bar{F}}\, dV_0 \tag{7}$$

Noting that

$$\delta\widetilde{F}_{ij} = \frac{\partial(\delta\widetilde{u}_i)}{\partial X_j} = \frac{\partial(\delta\widetilde{u}_i)}{\partial X_k}\ \frac{\partial x_k}{\partial X_j} = L_{ik}\,\widetilde{F}_{kj}\,\delta t \tag{8}$$

where $\bar{\bar{L}}\partial\left(\frac{\dot{}}{u}\right)/\partial\bar{x}$ is the velocity gradient tensor, function of current positions $\bar{x}$, the following can be obtained after some algebra (see [11]):

$$W_2 = \int_V \left(\delta\bar{\bar{\sigma}} + \frac{\delta J}{J}\,\bar{\bar{\sigma}} - \bar{\bar{\sigma}}\left(\bar{\bar{L}}\right)^t \delta t\right) : \bar{\bar{L}}\,\delta t\,dV \tag{9}$$

If homogeneous conditions exist in volume V, the following straightforward expression of the second-order work holds in Lagrangian description:

$$W_2 = V\,\delta\Pi_{ij}\,\frac{\partial(\delta\widetilde{u}_i)}{\partial X_j}\ = V\,\delta\Pi_{ij}\,\delta\widetilde{F}_{ij} \tag{10}$$

When the two configurations C_0 and C coincide at time t (updated Lagrangian configuration), $\bar{\bar{L}}\ \ \delta t = \delta\bar{\bar{F}}$, and according to Eq. (9), the expression of the second-order work in Eulerian description is as follows:

$$W_2 = V\,\delta\bar{\bar{\sigma}} : \bar{\bar{D}}\,\delta t + \delta V\,\bar{\bar{\sigma}} : \bar{\bar{D}}\,\delta t - V\,\bar{\bar{\sigma}}\left(\delta\bar{\bar{F}}\right)^t : \delta\bar{\bar{F}} \tag{11}$$

where $\bar{\bar{D}} = \left(\bar{\bar{L}} + \bar{\bar{L}}^t\right)/2$.

An important consequence of Eq. (11) is that the standard expression $W_2 = V\,\delta\bar{\bar{\sigma}} : \bar{\bar{D}}\,\delta t$ is generally not valid. This question will be considered in Section 3.

In the following, an updated Lagrangian configuration will be adopted: the current configuration stands as the reference configuration, $\bar{\bar{\Pi}} = \bar{\bar{\sigma}}$, $\bar{\bar{F}} = \bar{\bar{I}}$ and $J = 1$.

2.2. *Micromechanically based formulation*

We consider a homogeneous volume of granular material comprised of N grains (the homogeneity here refers to the material properties of grains, as well as to the texture—or fabric—of the granular assembly). Throughout the paper, 'p' will denote indiscriminately the grain (as a body) or enumerate a particular grain within the assembly such that $1 \le p \le N$. The shape of each grain 'p' is arbitrary. The total number of contacts at time t within the assembly is denoted N_c.

The system is assumed to be in equilibrium at a given time t under a prescribed external loading. Depending on the type of loading control, each grain 'p' belonging to the boundary ∂V of the considered volume is subjected to either a displacement (kinematic control) or an external force $\bar{f}^{\text{ext},p}$ (static control), possibly zero.

The second-order work, in its basic formulation, involves both incremental stress and strain. The stress within a granular assembly expresses the transmission of forces in granular materials. The transmission of forces in granular materials operates at contacts of adjoining grains, thereby resulting in a macroscopic average stress at the grain assembly level. The stress tensor in such a body of volume V in equilibrium under external forces $\bar{f}^{\text{ext},p}$ applied to the boundary particles 'p' of position $\bar{x}^p$ can be defined by the classical Love–Weber formula [12–15], that is,

$$\sigma_{ij} = \frac{1}{V}\ \sum_{p\in\partial V} f_i^{\text{ext},p}\ \ x_j^p \tag{12}$$

It is worth noting that Eq. (12) is not exact, as $\bar{x}^p$ should denote the location of the point where the external force $\bar{f}^{\text{ext},p}$ is applied, not the centre of gravity of grain 'p'. For specimens containing a sufficiently large number of grains (see [16]), this approximation is shown to be reasonably acceptable.

The aforementioned expression can be transformed as follows, by accounting for the inter-particle contact forces $\bar{f}^c$ [11]:

$$\sigma_{ij} = \frac{1}{V} \sum_{c=1}^{N_c} f_i^c \; l_j^c + \frac{1}{V} \sum_{p \in V} f_i^p \; x_j^p \tag{13}$$

where $\bar{l}^c$ is the branch vector relating the centres of contacting particles and $\bar{f}^p$ denotes the resultant force applied to the particle 'p'. In the absence of inertial effects or when all particles are in static equilibrium, the second term in Eq. (13) vanishes. However, this term may subsist in the presence of internal dynamical effects that arise from local force imbalances, even if the whole granular body may be in equilibrium macroscopically.

Thus, by differentiating Eq. (13) and by combining with Eq. (1), the following relation is obtained (see [5], for more details):

$$W_2 = \sum_{p,q} \delta f_i^c \; \delta l_i^c + \sum_{p \in V} \delta f_i^p \; \delta x_i^p \tag{14}$$

As specified in Nicot *et al*. [11], the creation or the deletion of contacts is accounted for in this approach. The symbol $\sum_{p,q}$ denotes the summation over p and q varying over $[1,\ N]$ with $q \leq p$, and c refers to the contacting pair $(p,\ q)$. In the absence of incremental unbalanced force and in quasi-static regime, as will be the case in the following sections, Eq. (14) simplifies into

$$W_2 = \sum_{p,q} \delta f_i^c \; \delta l_i^c \tag{15}$$

In what follows, Eq. (15) is investigated using a micromechanically based model. Further conclusions are drawn from simulations run with a discrete element method.

3. MULTISCALE APPROACH AND SECOND-ORDER WORK

The previous results derived from a general theoretical approach are now further investigated using a two-dimensional micromechanically based constitutive relation. Even though no inertial effect is accounted for in the constitutive model proposed, it is of interest to investigate, in the absence of unbalanced forces, the validity of the multiscale expression of the second-order work (Eqs (14) and (15)). First, the *H*-microdirectional model [6], which relates the incremental stress $\delta\bar{\bar{\sigma}}$ to the incremental strain $\delta\bar{\bar{\varepsilon}}$, is briefly reviewed. This model was developed within a multiscale approach, in continuity with a previously developed microdirectional model Nicot and Darve [17, 18]. The introduction of an intermediate scale between the particle scale and the specimen scale (REV) is one of the innovative features of the model.

3.1. The H-microdirectional model

In this section, a general two-dimensional reference frame $(\bar{x}_1,\ \bar{x}_2)$ is introduced, in which both stress and strain are calculated. Furthermore, the axes $\bar{x}_1$ and $\bar{x}_2$ are chosen to coincide with the principal directions of the macroscopic strain tensor $\bar{\bar{\varepsilon}}$, which are first assumed not to rotate: $\bar{\bar{\varepsilon}} = \begin{bmatrix} \varepsilon_1 & 0 \\ 0 & \varepsilon_2 \end{bmatrix}$.

It has been shown (see e.g. [19, 20]) that the local kinematics of a granular mass cannot be described only through the contact between two adjoining particles. In other words, the relevant local kinematic variable is not the relative displacement between adjoining grains. Instead, a mesoscopic scale has to be introduced, at which a kinematic (tensorial) variable can be formulated. With a view to

developing a micromechanically based constitutive relation, this mesostructure has to be defined such that it allows a complex enough kinematics to take place, while at the same time involving analytically tractable derivations. Thus, in this model, the granular assembly is described by a distribution of regular, symmetric hexagonal arrangements of identical spherical grains with a radius r_g, oriented along the symmetry direction $\vec{n}$ (Figure 1). Many other arrangements can be found in real granular assemblies. The hexagonal packing has the merit of giving rise to complex kinematic mechanisms, including local dilatant or contractant behaviour.

Moreover, it is worth emphasizing that the strain of each branch vector between adjoining particles of the hexagon does not derive from $\bar{\bar{\varepsilon}}$. In contrast, the affine assumption can reasonably be applied to describe the strain of elementary sets containing a few grains [21, 22]. The deformation of each hexagon is therefore assumed to derive from the macroscopic strain on the specimen scale as follows (Figure 2):

- Extension along direction $\vec{n}$: $\delta\varepsilon_{ij}\, n_i\, n_j$
- Extension along direction $\vec{t}$: $\delta\varepsilon_{ij}\, t_i\, t_j$
- Distortion between directions $\vec{n}$ and $\vec{t}$: $\delta\varepsilon_{ij}\, n_i\, t_j$

As the first approximation, and for the purpose of this paper, the distortion will be neglected. As a result, the affine assumption is only partially applied. Neglecting distortion is motivated by the fact that we impose that each hexagon keeps the hexagonal shape over any loading path. This constraint involves that no shearing occurs between grains 2 and 3, and 5 and 6. The deformation of each hexagon can be characterized by the change in lengths l_1 and l_2. Extension along both directions $\rightarrow n$ and $\rightarrow t$ can be expressed as

$$\delta l_1 = -l_1\ \ \delta\varepsilon_{ij}\ \ n_i\ \ n_j = -l_1\ \ \left(\delta\varepsilon_1\ \ {n_1}^2 + \delta\varepsilon_2\ \ {n_2}^2\right) \tag{16a}$$

$$\delta l_2 = -l_2\ \ \delta\varepsilon_{ij}\ \ t_i\ \ t_j = -l_2\ \ \left(\delta\varepsilon_1\ \ {t_1}^2 + \delta\varepsilon_2\ \ {t_2}^2\right) \tag{16b}$$

In addition, no rolling is assumed to affect particles. This assumption is undoubtedly questionable for spherical shaped grains, where particle rolling acts as an important ingredient of the deformational processes [23]. However, it seems to be reasonable for real granular soil materials where actual grains are angular with multiple facets Oda *et al*. [24, 25].

Let N_1 denote the normal component and T_1 the tangential component of the contact force applied by grain 2 on grain 1 and N_2 the normal component of the contact force applied by grain 3 on grain 2 (the tangential component being zero). The separating distances d_1 and d_2 are the branch lengths, whereas α is the opening angle of each hexagon (refer to Figure 2 for the notations). As a result of the assumed external forces applied to the hexagonally arranged particles (Figure 2), the following relation can be derived:

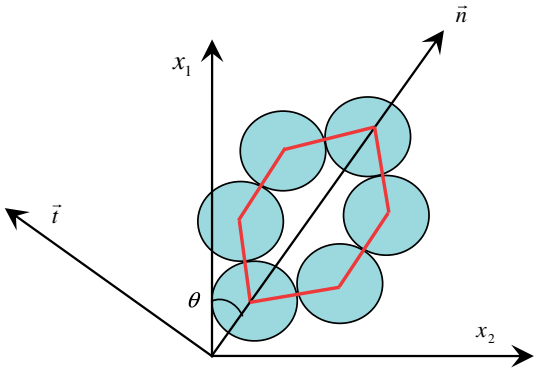

Figure 1. Hexagonal set of contacting particles.

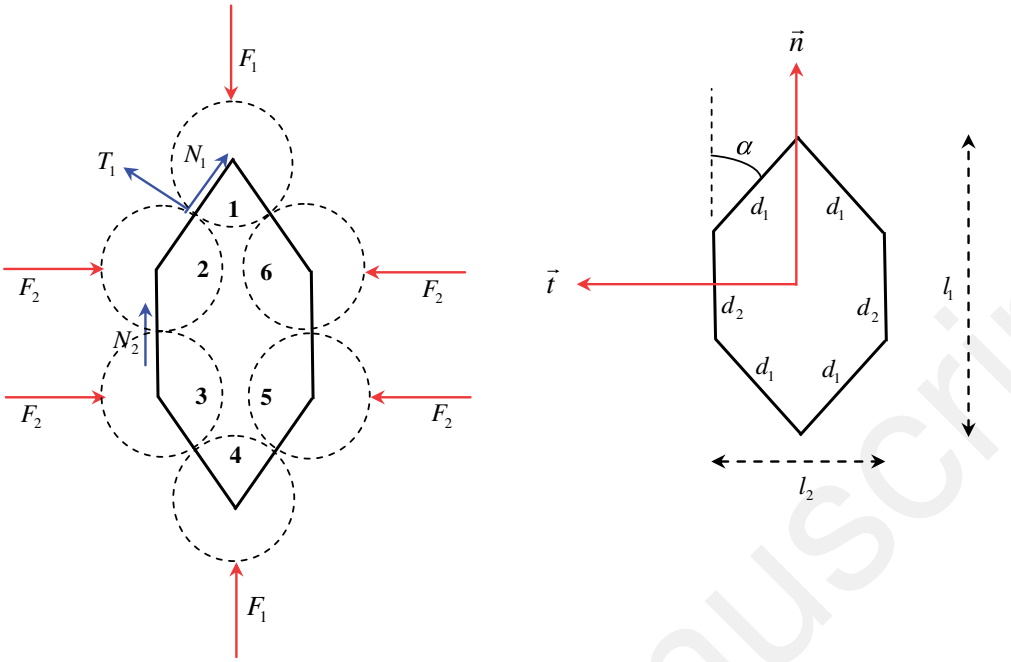

Figure 2. Geometrical description, external forces applied to each hexagon and contact forces.

$$N_2 = N_1 \ \cos\alpha + T_1 \ \sin\alpha \tag{17}$$

In addition, the following geometrical relations hold:

$$l_1 = d_2 \ + 2d_1 \ \cos\alpha \tag{18}$$

$$l_2 = 2d_1 \ \sin\alpha \tag{19}$$

Moreover, the local behaviour can be described properly using an elastic–plastic mechanical model relating both the local normal and tangential forces to both the local normal and tangential relative displacements. This model includes a Mohr–Coulomb criterion and can be expressed under the following incremental formalism, which introduces a normal elastic stiffness k_n and a tangential elastic stiffness k_t, both constant, and a local friction angle ϕ_g:

$$\delta N_1 = -k_n \ \delta d_1 \tag{20}$$

$$\delta N_2 = -k_n \ \delta d_2 \tag{21}$$

$$\delta T_1 = \min \left\{ |T_1 + k_t \ d_1 \ \delta\alpha|, \ \tan\phi_g \ (N_1 + k_n \ \delta d_1) \right\} \ \xi - T_1 \tag{22}$$

where ξ is the sign of the quantity $T_1 + k_t \, d_1 \, \delta\alpha$.

The expression of the macroscopic Cauchy stress tensor (that coincides with the Piola–Kirchoff stress tensor $\bar{\bar{\Pi}}$ in updated Lagrangian configuration) is obtained by averaging all contact forces over the overall specimen of volume V (Love–Weber formula), that is,

$$\bar{\bar{\sigma}} = \frac{1}{V} \int \omega_e(\bar{n}) \ \bar{\bar{P}}^{-1} \begin{bmatrix} S_1 & 0 \\ 0 & S_2 \end{bmatrix} \bar{\bar{P}} \ d\theta \tag{23}$$

where $\bar{\bar{P}} = \begin{bmatrix} \cos\theta & -\sin\theta \\ \sin\theta & \cos\theta \end{bmatrix}$ is the transformation matrix from $(\bar{x}_1, \ \bar{x}_2)$ to $(\bar{n}, \ \bar{t})$ axes and $\omega_e(\bar{n})$ is the number of hexagons oriented along the direction $\bar{n} = \cos\theta \ \bar{x}_1 + \sin\theta \ \bar{x}_2$. The distribution of $\omega_e(\bar{n})$ makes modelling the microstructure of the specimen possible. In particular, according to the initial

distribution of $\omega_e(\bar{n})$, an initial fabric anisotropy can be accounted for. Hereafter, $\omega_e(\bar{n})$ is assumed to remain constant. However, this constraint can be removed, and the change in $\omega_e(\bar{n})$ over the loading history can be modelled by incorporating a suitable evolution law (see e.g. [26, 27, 24, 28, 17]). Without any other specification, any integral $\int f(\bar{n})\ d\theta$ is computed over the range $[0,\ \pi]$, so that all hexagon orientations $\bar{n} = \cos\theta\ \bar{x}_1 + \sin\theta\ \bar{x}_2$ are considered. The terms S_1 and S_2 are given by the relations (see [6]):

$$S_1 = 4N_1\ d_1\ \cos^2\alpha + 4T_1\ d_1\ \cos\alpha\ \sin\alpha + 2N_2\ d_2 \tag{24}$$

and

$$S_2 = 4N_1\ d_1\ \sin^2\alpha - 4T_1\ d_1\ \cos\alpha\ \sin\alpha \tag{25}$$

3.2. Analytical derivation of the incremental stress

Both Eqs (24) and (25) can be expressed differently by taking advantage of relations (17)–(19). Because $S_1 = 4d_1\ \cos\alpha\ (N_1\ \cos\alpha + T_1\ \sin\alpha) + 2N_2\ d_1$, it follows that

$$S_1 = 2(N_1\ \cos\alpha + T_1\ \sin\alpha)\ l_1 = 2N_2\ l_1 \tag{26}$$

Likewise,

$$S_2 = 2l_2\ (N_1\ \sin\alpha - T_1\ \cos\alpha) \tag{27}$$

Thus, the differentiation of Eq. (23) yields

$$\delta\bar{\bar{\sigma}} = -\frac{\delta V}{V}\ \bar{\bar{\sigma}} + \frac{1}{V}\ \int \omega_e(\bar{n})\ \bar{\bar{P}}^{-1} \begin{bmatrix} \delta S_1 & 0 \\ 0 & \delta S_2 \end{bmatrix} \bar{\bar{P}}\ d\theta \tag{28}$$

with

$$\delta S_1 = 2\delta N_2\ l_1 + 2N_2\ \delta l_1 \tag{29}$$

$$\delta S_2 = 2l_2\ \delta(N_1\ \sin\alpha - T_1\ \cos\alpha) + 2\delta l_2\ (N_1\ \sin\alpha - T_1\ \cos\alpha) \tag{30}$$

As a consequence, one recovers the fact that the incremental Cauchy stress tensor is composed of three tensors, namely

- The tensor ($\bar{\bar{T}}_1$), which corresponds to the incremental Lagrangian stress ($\delta\bar{\bar{\Pi}}$) and which accounts for the change in forces acting in a fixed configuration, $\bar{\bar{T}}_1 = \frac{1}{V} \int \omega_e(\bar{n})\ \bar{\bar{P}}^{-1} \begin{bmatrix} 2\delta N_2\ l_1 & 0 \\ 0 & 2l_2\ (\delta(N_1\ \sin\alpha) - \delta(T_1\ \cos\alpha)) \end{bmatrix} \bar{\bar{P}}\ d\theta.$
- The term ($\bar{\bar{T}}_2$), accounting for the change in the bulk volume, $\bar{\bar{T}}_2 = -\frac{\delta V}{V}\ \bar{\bar{\sigma}} = -\frac{\delta V}{V}\ \bar{\bar{\Pi}}$.
- The transport term ($\bar{\bar{T}}_3$), related to the change in the geometrical configuration with constant forces, $\bar{\bar{T}}_3 = \frac{1}{V}\ \int \omega_e(\bar{n})\ \bar{\bar{P}}^{-1} \begin{bmatrix} 2N_2\ \delta l_1 & 0 \\ 0 & 2\delta l_2\ (N_1\ \sin\alpha - T_1\ \cos\alpha) \end{bmatrix} \bar{\bar{P}}\ d\theta$

It can be shown (Appendix A) that

$$\bar{\bar{T}}_3 = \bar{\bar{\Pi}}\ \delta\bar{\bar{\varepsilon}} + (\delta\varepsilon_1 - \delta\varepsilon_2)\ \bar{\bar{\chi}} \tag{31}$$

with $\bar{\bar{\chi}} = \frac{1}{V}\ \int \omega_e(\bar{n}) \begin{bmatrix} -\sin\theta\ \cos\theta\ (S_2 + S_1) & \cos^2\theta\ S_1 - \sin^2\theta\ S_2 \\ \cos^2\theta\ S_2 - \sin^2\theta\ S_1 & \sin\theta\ \cos\theta\ (S_2 + S_1) \end{bmatrix} \sin\theta\ \cos\theta\ d\theta$

It is checked from numerical computations that the terms χ_{ij} are negligible with respect to Π_{ij}. Furthermore, in small strains, in the absence of rotation of the specimen and in the principal

axes of $\delta\bar{\bar{\varepsilon}}$, $\delta\bar{\bar{\varepsilon}} = \delta\widetilde{\bar{\bar{F}}} = \left(\delta\bar{\bar{\widetilde{F}}}\right)^t$. Consequently, Eq. (6) is recovered with the *H*-microdirectional model, which can be regarded as a proof of consistency for this model.

3.3. Directional analysis of the incremental stress

In this section, the nature of the incremental stress is investigated for different directions of incremental strain probes. For this purpose, after an initial drained biaxial loading at a confining pressure $\sigma_2 = 200$ kPa, a directional analysis is performed [29], whereby incremental strain probes are imposed along all the directions of the incremental strain space, and the incremental stress response is computed (Figure 3). As the analysis is carried out in the principal (strain and stress) axes, it is worth mentioning that no simple shearing is considered.

The simulations were carried out using the numerical parameters reported in Table I. The distribution of $\omega_e(\vec{n})$ is chosen to be uniform. Moreover, the opening angle α (Figure 2) is assumed to be uniformly distributed over all the directions $\vec{n}$. Thus, $\alpha(\vec{n}) = \alpha_o$ whatever the direction $\vec{n}$. As investigated in [6], the value of $\alpha(\vec{n})$ can be mapped to the void ratio related to the hexagons oriented along the direction $\vec{n}$. However, this local void ratio should not be confused with the macroscopic void ratio applying to the whole specimen. In the simulation proposed, the notion of macroscopic void ratio cannot be defined, even though the constitutive features of both loose and dense specimens can be retrieved depending on the value of α_o [6].

The evolution of the deviatoric stress $q = \sigma_1 - \sigma_2$ with respect to the axial strain is illustrated in Figure 4, whereas the corresponding volumetric behaviour is given in Figure 5. The directional analysis was carried out at a state indicated on the curve (point A) and corresponding to a deviatoric ratio $\eta = q/p = 1.029$. For each incremental strain probe, the incremental stress response was normalized ($\delta\bar{\bar{\sigma}}/\|\delta\bar{\bar{\sigma}}\|$), and the contribution of the three different components was analysed for both the axial (Figure 6) and the lateral (Figure 7) directions. As seen in these figures, the contribution of both the volume change term (T_2) and the configuration change term (T_3) is negligible when the loading direction belongs to the elastic tensorial zone[§] but cannot be omitted (especially for the configuration change term T_3, the influence of which is quite significant) in the plastic tensorial zone[¶] (for α_σ ranging between 70° and 250°).

As a consequence, if a Eulerian description is adopted, the incremental stress should not be reduced to the force change term (T_1) because the contribution of the change in the configuration can be substantial if the specimen is loaded along a direction belonging to the plastic tensorial zone. As a result, the second-order work departs from the standard expression $W_2 = V\ \delta\bar{\bar{\sigma}} : \bar{\bar{D}}\ \delta t$, requiring a change in geometry terms to be accounted for, as will be established in the next section.

3.4. Directional analysis of the second-order work

The macroscopic second-order work is given in a straightforward manner in Lagrangian description as $W_2 = V\ \delta\Pi_{ij}\ \delta\widetilde{F}_{ij}$. Using the *H*-microdirectional model, and noting that

$$\delta\bar{\bar{\Pi}} = \frac{1}{V} \int \omega_e(\bar{n})\ \bar{\bar{P}}^{-1} \begin{bmatrix} 2\delta N_2\ l_1 & 0 \\ 0 & 2l_2\ (\delta(N_1\ \sin\alpha) - \delta(T_1\ \cos\alpha)) \end{bmatrix} \bar{\bar{P}}\ \mathrm{d}\theta \tag{32}$$

it follows that

$$W_2 = \int \omega_e(\bar{n})\ \bar{\bar{P}}^{-1} \begin{bmatrix} 2\delta N_2\ l_1 & 0 \\ 0 & 2l_2\ (\delta(N_1\ \sin\alpha) - \delta(T_1\ \cos\alpha)) \end{bmatrix} \bar{\bar{P}} : \delta\bar{\bar{\varepsilon}}\ \mathrm{d}\theta \tag{33}$$

[§]The elastic tensorial zone encompasses all the stress (or strain) incremental directions along which the material behaves elastically. Along these directions, no sliding occurs within the hexagons.

[¶]The plastic tensorial zone encompasses all the stress (or strain) incremental directions along which the material behaves plastically (sliding occurs along some contacts).

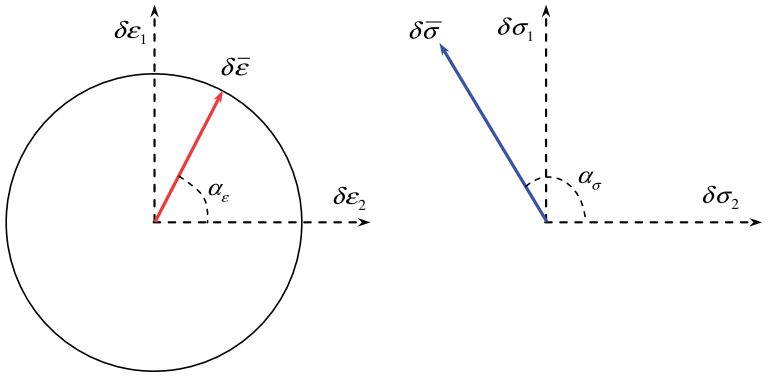

Figure 3. Directional analysis: strain probes and stress responses.

Table I. Numerical simulation: constitutive parameters and initial conditions.

Initial isotropic stress (kPa)	k_n (kN/m)	k_t (kN/m)	ϕ_g (deg)	r_g (m)	α_o (deg)
200	1000	500	20	0.001	42.8

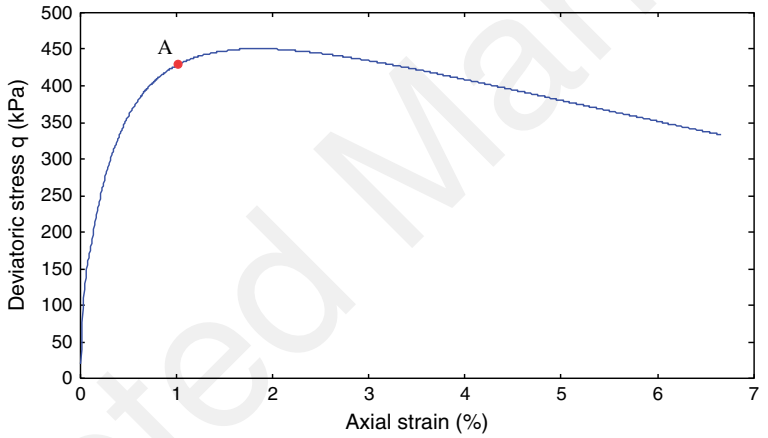

Figure 4. Response of a drained biaxial test using the *H*-microdirectional model. Evolution of the deviatoric stress versus the axial strain.

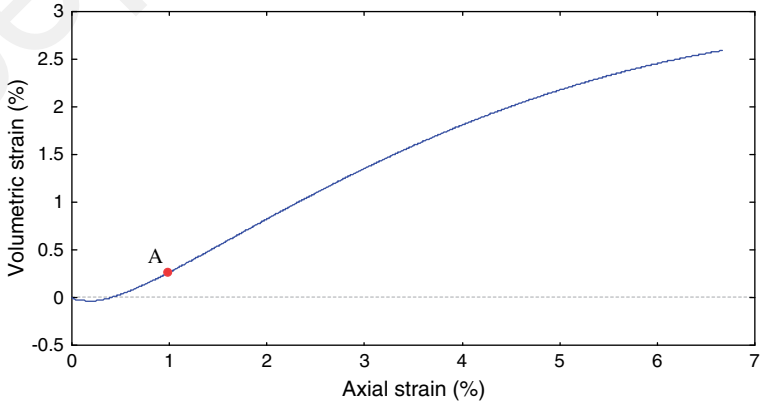

Figure 5. Response in a drained biaxial test using the *H*-microdirectional model. Evolution of the volumetric strain versus the axial strain.

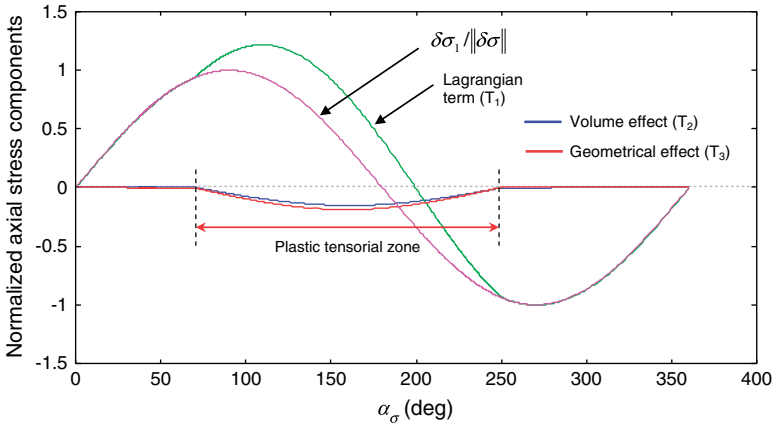

Figure 6. Influence of the different components of the normalized incremental axial stress.

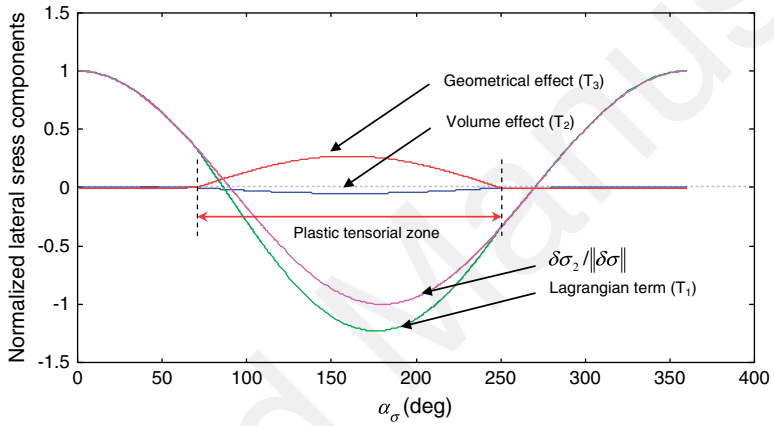

Figure 7. Influence of the different components of the normalized incremental lateral stress.

Furthermore, working out

$$\bar{\bar{P}}^{-1}\begin{bmatrix} 2\delta N_2\ l_1 & 0 \\ 0 & 2l_2\ (\delta(N_1\ \sin\alpha) - \delta(T_1\ \cos\alpha)) \end{bmatrix}\bar{\bar{P}} : \delta\bar{\bar{\varepsilon}} =$$

$$\begin{bmatrix} 2\delta N_2\ l_1 & 0 \\ 0 & 2l_2\ (\delta(N_1\ \sin\alpha) - \delta(T_1\ \cos\alpha)) \end{bmatrix} : \bar{\bar{P}}^{-1}\ \delta\bar{\bar{\varepsilon}}\ \bar{\bar{P}} \tag{34}$$

with

$$\bar{\bar{P}}^{-1}\ \delta\bar{\bar{\varepsilon}}\ \bar{\bar{P}} = \begin{bmatrix} \cos^2\theta\ \delta\varepsilon_1 + \sin^2\theta\ \delta\varepsilon_2 & \cos\theta\ \sin\theta\ (\delta\varepsilon_1 - \delta\varepsilon_2) \\ \cos\theta\ \sin\theta\ (\delta\varepsilon_1 - \delta\varepsilon_2) & \sin^2\theta\ \delta\varepsilon_1 + \cos^2\theta\ \delta\varepsilon_2 \end{bmatrix} \tag{35}$$

and accounting for Eqs (16a) and (16b), Eq. (33) can be rewritten as

$$W_2 = \int \omega_e(\bar{n})\ w_2\ \mathrm{d}\theta \tag{36}$$

where $w_2 = 2\delta N_2\ \delta l_1 + 2(\delta(N_1\ \sin\alpha) - \delta(T_1\ \cos\alpha))\ \delta l_2$.

The expression of w_2 can be rearranged by taking Eqs (17)–(19) into account, that is,

$$w_2 = 2\delta N_2 \;\; \delta d_2 + 4(\delta(N_1 \;\; \sin\alpha) - \delta(T_1 \;\; \cos\alpha)) \;\; \delta(d_1 \;\; \sin\alpha)$$

$$+4(\delta(N_1 \;\; \cos\alpha) + \delta(T_1 \;\; \sin\alpha)) \;\; \delta(d_1 \;\; \cos\alpha) \tag{37}$$

Thus, w_2 corresponds exactly to the term $\sum_{c=1}^{N_c} \delta f_i^c \;\; \delta l_i^c$ evaluated for a given hexagon. As Eq. (36) expresses the continuous description of local second-order work by replacing the discrete summation over all the contacts by an integral over all the directions of the physical space, the macroscopic second-order work equals the term $\sum_{c=1}^{N_c} \delta f_i^c \;\; \delta l_i^c$ evaluated for the whole assembly. As in the *H*-microdirectional model, no inertial effect is accounted for, the term $\sum_{p \in V} \delta f_i^p \;\; \delta x_j^p$ is zero and the basic relation $W_2 = \sum_{p,q} \delta f_i^c \;\; \delta l_i^c$ is therefore perfectly verified, confirming the validity of Eq. (14) in the absence of unbalanced forces.

Another aspect worth investigating by considering the *H*-microdirectional model concerns Eq. (11), which may be written in this particular case as

$$W_2 = V \;\; \delta\bar{\bar{\sigma}} : \delta\bar{\bar{\varepsilon}} \;\; + \;\; \delta V \;\; \bar{\bar{\sigma}} : \delta\bar{\bar{\varepsilon}} - V \;\; \bar{\bar{\sigma}} \;\; (\delta\bar{\bar{\varepsilon}}) : \;\; \delta\bar{\bar{\varepsilon}} \tag{38}$$

With the decomposition of the Cauchy stress tensor given in Eq. (6), the second-order work is thereby the sum of three terms. By using the directional analysis presented in Section 3.3, the relative contribution of each term can be investigated ($\sigma_2 = 200$ kPa, $\eta = 1.029$). Computation of the incremental stress for each incremental strain probe direction determines the normalized second-order work: $W_2 = \delta\bar{\bar{\Pi}} : \delta\bar{\bar{\varepsilon}} / \left\| \delta\bar{\bar{\Pi}} \right\| / \|\delta\bar{\bar{\varepsilon}}\|$. For convenience, a polar plot is chosen [30], constituted of points of coordinates $(\cos\alpha_\sigma \;\; (0.5 + W_2), \;\; \sin\alpha_\sigma \;\; (0.5 + W_2))$, where $\tan\alpha_\sigma = \delta\sigma_1 / \delta\sigma_2$. When the second-order work takes negative values, the polar diagram crosses the dashed circle of radius $r = 0.5$. Figure 8 shows that the second-order work takes negative values along the stress directions contained within a cone, as reported in the literature by many authors (see e.g. [1, 31, 32]). The

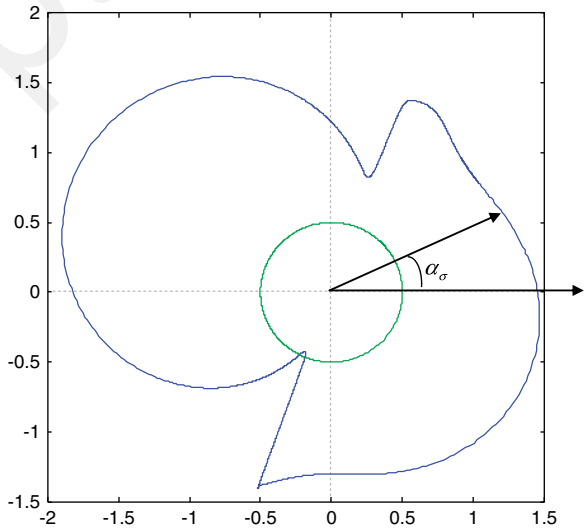

Figure 8. Polar diagram of the normalized second-order work.

negative values of the macroscopic second-order work are essentially observed within the third quadrant, corresponding to $\delta\sigma_1 < 0$ and $\delta\sigma_3 < 0$ in the stress incremental space (in some cases, negative values of the second-order work can also be observed within the first quadrant; [1]). This result can be related to the simple, discrete case of two contacting frictional bodies (the sliding condition corresponds to the standard Coulomb criterion). It was shown [8] that the local second-order work associated with this pair of contacting bodies takes negative values when both normal and tangential components δF_c^n and δF_c^t of the incremental contact force are negative. Locally, on the contact scale, the stress state descends the Coulomb line.

The contributions of the different normalized terms $W_2^\sigma = \delta\bar{\bar{\sigma}} : \delta\bar{\bar{\varepsilon}} / \left\| \delta\bar{\bar{\Pi}} \right\| / \|\delta\bar{\bar{\varepsilon}}\|$, $W_2^V = (\delta V/V)\ \bar{\bar{\sigma}} : \delta\bar{\bar{\varepsilon}} / \left\| \delta\bar{\bar{\Pi}} \right\| / \|\delta\bar{\bar{\varepsilon}}\|$ and $W_2^g = -\bar{\bar{\sigma}}\ (\delta\bar{\bar{\varepsilon}}) :\ \ \delta\bar{\bar{\varepsilon}} / \left\| \delta\bar{\bar{\Pi}} \right\| / \|\delta\bar{\bar{\varepsilon}}\|$ are analysed in Figure 9. The term W_2^σ is related to the change in the Cauchy stress tensor, the term W_2^V is related to the change in volume and W_2^g is related to geometrical changes (see [8]).

In line with the conclusions drawn for the incremental stress components, the contributions of both terms W_2^V and W_2^g are negligible inside the elastic tensorial zone but become significant in the plastic tensorial zone. It should be noted that the so-called instability cone in which the second-order work takes negative values is more developed for the term W_2^σ than for W_2. As a consequence, the detection of instability could be altered if based on the vanishing of W_2^σ rather than W_2. In fact, an examination of Figure 9 reveals that the second-order work (W_2^σ or W_2) takes negative values close to the boundary of the plastic tensorial zone. As a consequence, the contribution of geometrical effects is less sensitive. This is confirmed by the analysis of the bifurcation domain boundary computed from the first vanishing of W_2^σ or W_2. For a given confining pressure, the lower boundary of the bifurcation domain is reached for the lowest deviatoric stress at which the second-order work vanishes (first occurrence of an unstable direction). The upper boundary coincides with the classical Mohr–Coulomb surface.

As seen in Figure 10, the location of the lower boundary of the bifurcation domain is nearly the same when computed from the first vanishing of W_2^σ or computed from the first vanishing of W_2 (even though the domain corresponding to W_2^σ is slightly larger). In conclusion, an accurate computation of the second-order work requires using the Piola–Kirchoff stress tensor (W_2), instead of the Cauchy stress tensor (W_2^σ). However, in so far as the H-microdirectional is considered, the detection of instability seems not to be affected by this distinction.

As seen in Figure 11, the tangential term W_2^t contributes, by taking negative values, to the vanishing of the second-order work, whereas the normal term W_2^n is always positive—as expected, because contacts behave elastically along the normal direction. It is worth noting the close analogy between these results obtained with a micromechanical model and those from a discrete element model [33–35].

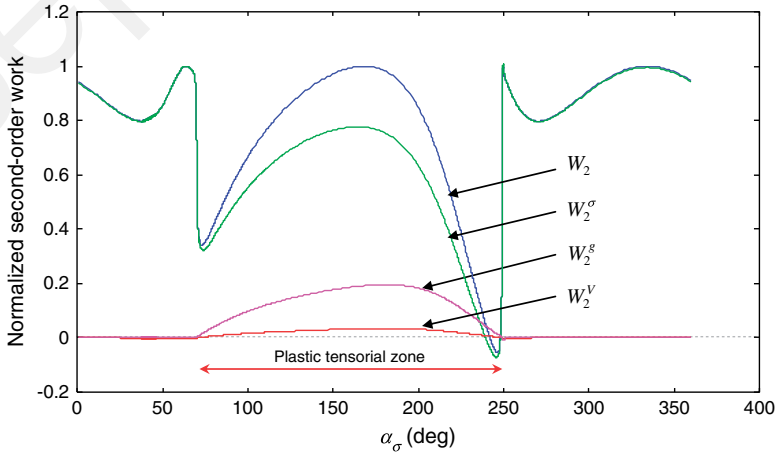

Figure 9. Contribution of the different components of the second-order work.

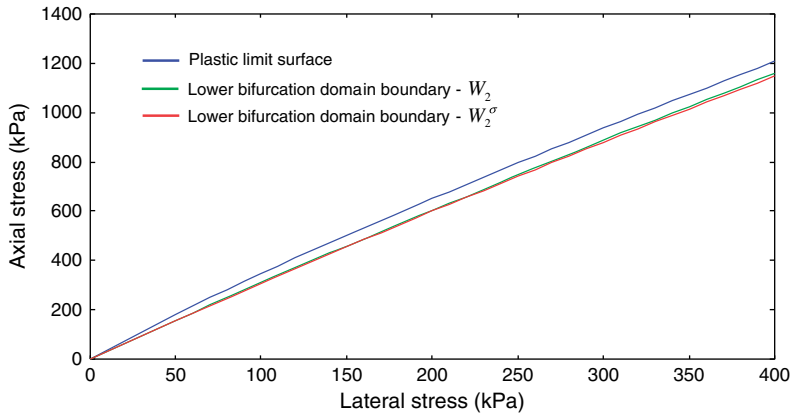

Figure 10. Boundary of the bifurcation domain.

4. NUMERICAL INVESTIGATION WITH A DISCRETE ELEMENT METHOD

In this section, a discrete element method-based model is proposed to check if any agreement with the multiscale approach using the *H*-microdirectional model can be worked out and how far the term $\sum_{p,q} \delta f_i^c \delta l_i^c$ (Eq. (15)) can approximate the vanishing of the macroscopic second order, thereby predicting failure in granular materials.

The numerical simulations presented in this section were carried out using 'Yade' software [7] based on the discrete element method [36]. Because DEM models are dealt with here, all the infinitesimal quantities denoted by δ will be denoted as Δ to define a finite increment computed between two consecutive numerical time steps.

A very dense two-dimensional specimen is considered, consisting of 12 000 disks of unit length enclosed within four frictionless walls (Figure 12). The disks can translate in the $\bar{x}$ and $\bar{y}$ directions and rotate around the $\bar{z}$ axis, whereas both translation along the $\bar{z}$ axis and rotations around the $\bar{x}$ and $\bar{y}$ axes are blocked. The disk radii are uniformly distributed and range from 3 to 14 mm.

The inter-particular contact model is defined by both a normal stiffness k_n and a tangential stiffness k_t such as $k_n/D = 32$ (GPa) and $k_t/k_n = 0.42$, where D is the mean diameter of the particles. Moreover, because the material is assumed to be cohesionless, only compressive normal forces are permitted; otherwise, the contact opens. Furthermore, the contact model obeys the Coulomb friction law; the tangential component f_c^t of the contact force $\vec{f}_c$ cannot exceed μf_c^n, where f_c^n is the normal component of the contact force, $\mu = \tan(\phi)$ is the friction coefficient and ϕ is the inter-particular angle of friction set here equal to 35°.

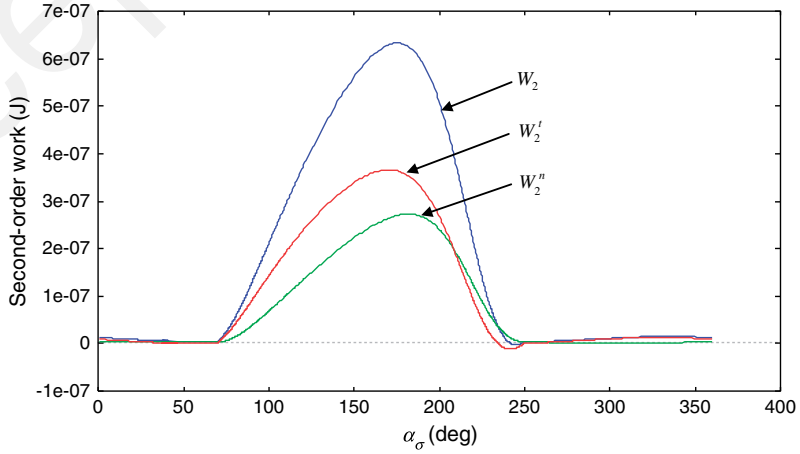

Figure 11. Second-order work: influence of the normal and tangential components.

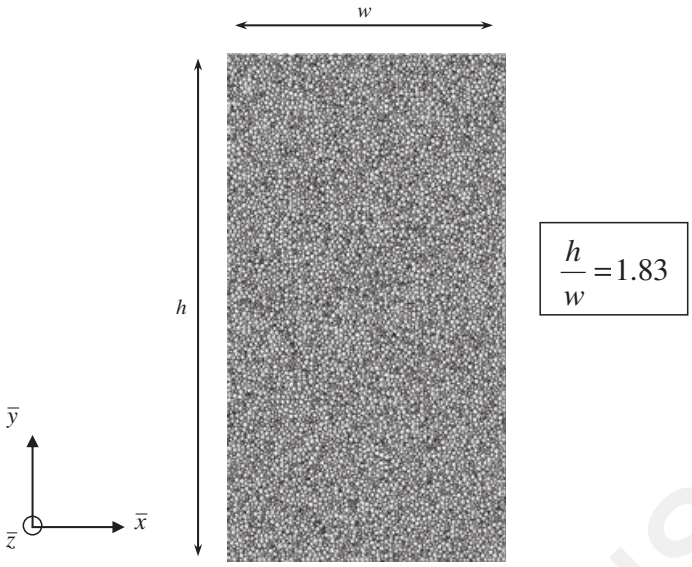

Figure 12. View of the granular assembly used in the discrete element model.

The parameters used in the DEM simulations (k_n, k_t, μ) were calibrated to fit with the results obtained with the *H*-microdirectional model over the drained biaxial test under 200 kPa of confining pressure.

The specimen is compacted by advancing the walls until the isotropic state is reached; at this stage, the confining pressure is equal to 200 kPa (in accordance with the *H*-microdirectional model), and the porosity is equal to 0.16.

A drained biaxial test is then performed by applying a constant strain rate $\dot{\varepsilon}_1 = 0.01\ s^{-1}$ in the axial direction $\bar{y}$, whereas the lateral walls are adjusted at every time step to maintain the lateral pressure constant.

In this context, the principal directions of both stress and strain tensors are fixed and coincide with the axial (1) and the lateral (2) directions.

The variation of the stress deviator $q = \sigma_1 - \sigma_2$ and the volumetric deformation $\varepsilon_v = \varepsilon_1 + \varepsilon_2$ in terms of the axial strain ε_1 are reported, respectively, in Figures 13 and 14. As a result of the calibrating of the parameters (k_n, k_t, μ) used in the DEM simulations, a good agreement (from both qualitative and quantitative points of view) is observed between the discrete element and the *H*-micromechanical models for the variation of the stress deviator (at least until the peak); some slight differences concern in particular the amounts of axial and volumetric strains corresponding to the contracting

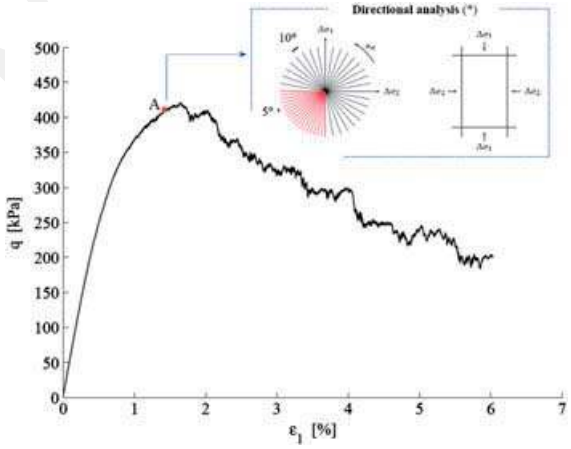

Figure 13. Response of a drained biaxial test using the discrete element model. Variation of the deviatoric stress in terms of the axial strain. (*) The directional analysis is performed at the stress state defined by A; stress probes are carried out at 5° intervals in the third quarter of the incremental stress space where the cone of instability is assumed to be found and 10° intervals elsewhere.

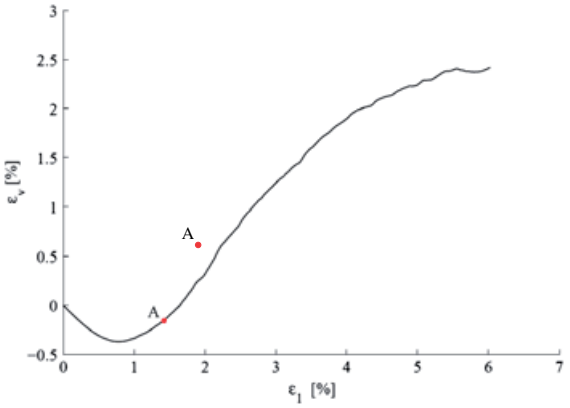

Figure 14. Response of a drained biaxial test using the discrete element model. Variation of the volumetric strain in terms of the axial strain.

phase, which are noticeably larger in the DEM model (Figures 4 and 13; Figures 5 and 14). Likewise, the behaviour in the softening regime (the descending branch after the deviatoric stress peak) is different. The softening behaviour is much more pronounced with the DEM model. In fact, localizations may occur after the peak, which is observed with the DEM model and of course not with the *H*-micromechanical model. Thus, only the purely constitutive softening regime can be accurately simulated with this analytical model.

Also, at the softening regime, the discrete element model loses strength in the axial direction faster than the *H*-microdirectional model, and this is due to sudden particle rearrangement at and after failure leading to instantaneous falls followed by instantaneous jumps of the axial stress when strength is resumed. This scenario is not capable of occurring in the *H*-microdirectional model because the softening regime is continuous and smooth (Figure 4).

Directional analysis is then performed at the stress state corresponding to the point A in Figure 13. At this loading state, chosen just before the peak in accordance with the previous analysis run from the *H*-microdirectional model, the stress ratio is $\eta = \frac{q}{p} = 1.029$. Stress probes of magnitude $\|\Delta\bar{\sigma}\| = 2.5$ kPa are carried out along 45 directions defined in the incremental stress space by the angle α_σ varying by an interval of 5° in the third quarter of the incremental stress space where the second-order work is assumed to vanish and 10° elsewhere (Figure 13).

Once the incremental strain corresponding to each stress probe is determined, the normalized second-order work W_2 is computed as described previously using the relation $W_2 = \Delta\bar{\sigma}.\Delta\bar{\varepsilon}/\|\Delta\bar{\sigma}\| \ \|\Delta\bar{\varepsilon}\|$. Figure 15 shows a polar diagram of W_2 plotted in the incremental stress space. A noticeable agreement with the diagram of W_2 of the *H*-microdirectional model shown in Figure 8 is observed; both second-order works vanish in the third quarter of the incremental stress space and have the same cone openings.

The second-order work from microscopic variables is computed by summing the scalar products $\Delta\bar{f}^c \cdot \Delta\bar{l}^c$ over all the contacts (including persisting, created and opening contacts), where $\Delta\bar{f}^c$ and $\Delta\bar{l}^c$ are the incremental variations experienced during each stress probe of the contact force and the branch vector joining the centres of the two contacting particles, respectively. Thereby, for each stress probe direction, the quantity $\sum_{p,q} \Delta f_i^c \Delta l_i^c$ is computed and then normalized with respect to $\|\Delta\bar{\sigma}\| \ \|\Delta\bar{\varepsilon}\|$.

Figure 16 shows a comparison between the normalized second-order works from both microscopic and macroscopic variables; an overall fit between both representative curves is observed.

In the plastic tensorial zone,[‖] the second-order work computed with macroscopic variables exceeds the term $\sum_{p,q} \Delta f_i^c \Delta l_i^c$ with noticeably more fluctuations on the curve representing the latter. This reflects

[‖]For a given strain increment, to compute both elastic and plastic parts, the following procedure is carried out: first, starting from a given stress–strain state, and given a stress increment $\Delta\bar{\sigma}$, the incremental strain response $\Delta\bar{\varepsilon}$ is computed; then, preventing sliding from occurring at the different contacts, from the same stress–strain state, the stress increment $\Delta\bar{\sigma}$ is imposed again, and the elastic response $\Delta\bar{\varepsilon}^e$ is computed. Incremental plastic strains are finally defined as $\Delta\bar{\varepsilon}^p = \Delta\bar{\varepsilon} - \Delta\bar{\varepsilon}^e$. Note that this procedure is similar to the one proposed by Calvetti *et al.*, 2003. The plastic tensorial zone corresponds to the range of stress directions along which the incremental plastic strains are not zero.

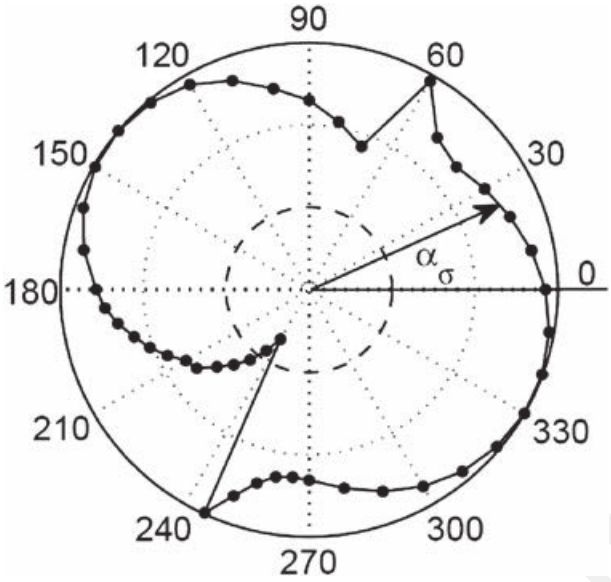

Figure 15. Polar diagram of the normalized second-order work computed after a directional analysis at the stress state defined by the point A.

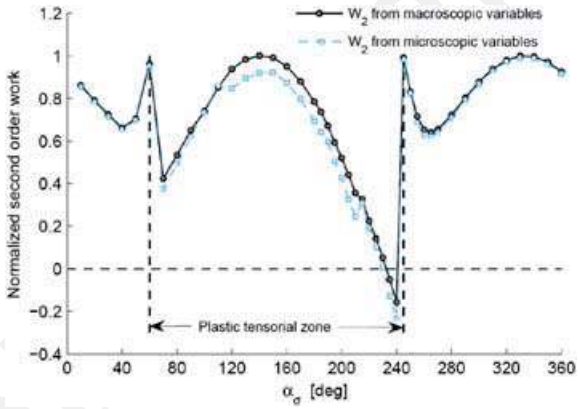

Figure 16. Comparison between the normalized second-order works from both macroscopic and microscopic variables.

the sensitivity of the microscopic second-order work towards fast particle positioning and rearrangement eligible to occur during incremental loading along certain directions in this zone. Consequently, this may affect the computed value of the second-order work because $\sum_{p,q} \Delta f_i^c \Delta l_i^c$ is computed from both initial (before stress probes (point A in Figure 13)) and final (after a stress probe in a given direction) stress states that are assumed to be at equilibrium. Thus, only contacts present at the initial state and those present at the final state are analysed. Thereby, the small difference between macroscopic and microscopic second-order works in the plastic tensorial zone stems from very short life contacts during loading.

Apart from this discrepancy, and compared with the results obtained from the *H*-microdirectional model (Figure 9), rather good agreement is observed even in the plastic tensorial zone, with the same slight superiority of the macroscopic W_2.

The *H*-microdirectional model seems to agree substantially well at both macroscopic and microscopic scales with the DEM model. Nevertheless, some discrepancies may arise as illustrated in Figure 17; the tangential component of the microscopic second-order work W_2^t computed in the

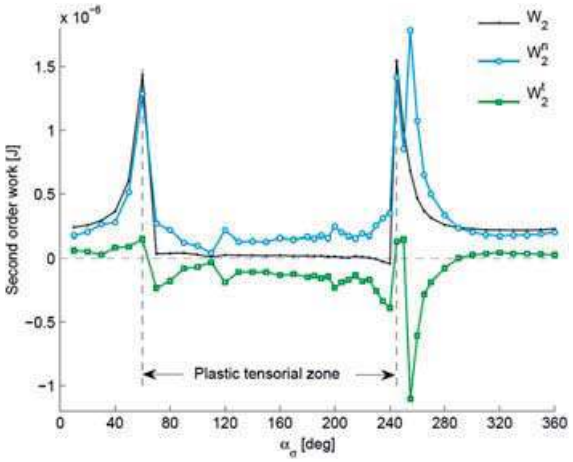

Figure 17. Contribution of the normal and tangential components of the second-order work from microscopic variables computed by the discrete element method model.

DEM model does not match the one computed from the *H*-microdirectional model. W_2^t takes negative values everywhere in the plastic tensorial zone with the DEM model, whereas it is positive along almost all directions but those corresponding to the cone opening with the *H*-microdirectional model. However, the striking point that can be put forward is that for both models, the vanishing of the second-order work stems from the negative values of the term W_2^t.

With the aforementioned analysis, the discrete element solution is shown to agree well with the micromechanical formalism of the second-order work. As highlighted from a multiscale approach using the *H*-microdirectional model, the main conclusion that has to be put forward is that the macroscopic second-order work can be fairly approximated by the term $\sum_{p,q} \delta f_i^c \delta l_i^c$.

5. CONCLUDING REMARKS

In this paper, we have explored the capability of the *H*-microdirectional model [6] to analyse the occurrence of instabilities detected by zero or negative values of the second-order work. This multiscale model is based on a homogenization procedure that involves successively three scales: a microscopic scale corresponding to the grain scale, a mesoscopic scale related to a hexagonal arrangement of grains and the entire assembly at the macroscopic scale. As such, even though the model does not include any dynamic mechanism, it allows the bridging of the different scales by expressing macroscopic variables in terms of microscopic variables. By using the concept of directional analysis, the *H*-microdirectional model shows the importance of the role played by changes in both geometrical configuration and the underlying microstructure in the computation of the second-order work.

Interestingly, direct simulations were run by using a discrete element method, to check (by comparison) the robustness of the *H*-microdirectional model. Despite that the two models are basically different (a discrete element method gives rise to direct numerical simulations, whereas the *H*-microdirectional model is a conceptual model), a fairly good convergence between the two methods has been observed. This can be regarded as a solid proof of consistency. In particular, the following convergent conclusions can be drawn:

- The boundary of the bifurcation domain experiences a very small sensitivity with respect to both the geometrical and microstructural changes.
- An instability cone is observed within the third quadrant (corresponding to $\delta\sigma_1 < 0$ and $\delta\sigma_3 < 0$ in the stress incremental space).
- The tangential part of the second-order work (term W_2^t) has a prominent influence on the existence of zero or negative values of the second-order work.

- A very good correspondence between both the microscopic and the macroscopic formulations of the second-order work was obtained, confirming that the macroscopic second-order work coincides with the sum of the microscopic second-order works (scalar product of incremental contact forces and incremental branch vectors), computed on all the contacts within the assembly, in the absence of inertial effects.

This investigation opens new perspectives in the understanding of the key mechanisms leading to the failure of granular specimens. In particular, extending this analysis for taking into account the influence of internal inertial mechanisms on the macroscopic destabilization of granular bodies appears as a major challenge.

APPENDIX A

The transport term ($\bar{\bar{T}}_3$) is now the subject of analysis. Because

$$\begin{bmatrix} 2N_2\ \delta l_1 & 0 \\ 0 & 2\delta l_2\ (N_1\ \sin\alpha - T_1\ \cos\alpha) \end{bmatrix} = \begin{bmatrix} 2N_2\ l_1 & 0 \\ 0 & 2l_2\ (N_1\ \sin\alpha - T_1\ \cos\alpha) \end{bmatrix} \begin{bmatrix} \dfrac{\delta l_1}{l_1} & 0 \\ 0 & \dfrac{\delta l_2}{l_2} \end{bmatrix} \tag{A1.1}$$

it follows that

$$\bar{\bar{T}}_3 = \frac{1}{V} \int \omega_e(\bar{n})\ \bar{\bar{P}}^{-1} \begin{bmatrix} S_1 & 0 \\ 0 & S_2 \end{bmatrix} \bar{\bar{P}}\ \bar{\bar{P}}^{-1} \begin{bmatrix} \dfrac{\delta l_1}{l_1} & 0 \\ 0 & \dfrac{\delta l_2}{l_2} \end{bmatrix} \bar{\bar{P}}\ \mathrm{d}\theta \tag{A1.2}$$

with $\bar{\bar{P}}^{-1} \begin{bmatrix} \dfrac{\delta l_1}{l_1} & 0 \\ 0 & \dfrac{\delta l_2}{l_2} \end{bmatrix} \bar{\bar{P}} = \begin{bmatrix} \cos^2\theta\ \dfrac{\delta l_1}{l_1} + \sin^2\theta\ \dfrac{\delta l_2}{l_2} & \left(\dfrac{\delta l_1}{l_1} - \dfrac{\delta l_2}{l_2}\right) \sin\theta\ \cos\theta \\ \left(\dfrac{\delta l_1}{l_1} - \dfrac{\delta l_2}{l_2}\right) \sin\theta\ \cos\theta & \sin^2\theta\ \dfrac{\delta l_1}{l_1} + \cos^2\theta\ \dfrac{\delta l_2}{l_2} \end{bmatrix}$

Taking advantage of Eqs (16a) and (16b), the following can be written:

$$\cos^2\theta\ \frac{\delta l_1}{l_1} + \sin^2\theta\ \frac{\delta l_2}{l_2} = \delta\varepsilon_1 - 2\cos^2\theta\ \sin^2\theta\ (\delta\varepsilon_1 - \delta\varepsilon_2) \tag{A1.3}$$

$$\sin^2\theta\ \frac{\delta l_1}{l_1} + \cos^2\theta\ \frac{\delta l_2}{l_2} = \delta\varepsilon_2 + 2\cos^2\theta\ \sin^2\theta\ (\delta\varepsilon_1 - \delta\varepsilon_2) \tag{A1.4}$$

$$\left(\frac{\delta l_1}{l_1} - \frac{\delta l_2}{l_2}\right) \sin\theta\ \cos\theta = \cos\theta\ \sin\theta\ \left(\cos^2\theta - \sin^2\theta\right)\ (\delta\varepsilon_1 - \delta\varepsilon_2) \tag{A1.5}$$

which leads to

$$\bar{\bar{P}}^{-1} \begin{bmatrix} \dfrac{\delta l_1}{l_1} & 0 \\ 0 & \dfrac{\delta l_2}{l_2} \end{bmatrix} \bar{\bar{P}} = \begin{bmatrix} \delta\varepsilon_1 & 0 \\ 0 & \delta\varepsilon_2 \end{bmatrix} + \sin\theta\ \cos\theta \begin{bmatrix} -\sin 2\theta & \cos 2\theta \\ \cos 2\theta & \sin 2\theta \end{bmatrix} (\delta\varepsilon_1 - \delta\varepsilon_2) \tag{A1.6}$$

Finally, by combining the aforementioned with Eq. (A1.2),

$$T_3 = \bar{\bar{\Pi}} \;\; \delta\bar{\bar{\varepsilon}} + (\delta\varepsilon_1 - \delta\varepsilon_2) \;\; \bar{\bar{\chi}} \tag{A1.7}$$

$$\text{with } \bar{\bar{\chi}} = \frac{1}{V} \int \omega_e(\bar{n}) \begin{bmatrix} -\sin\theta \;\; \cos\theta \;\; (S_2 + S_1) & \cos^2\theta \;\; S_1 - \sin^2\theta \;\; S_2 \\ \cos^2\theta \;\; S_2 - \sin^2\theta \;\; S_1 & \sin\theta \;\; \cos\theta \;\; (S_2 + S_1) \end{bmatrix} \sin\theta \;\; \cos\theta \;\; d\theta$$

ACKNOWLEDGEMENT

The authors would like to express their sincere thanks to the French Research Network MeGe (Multiscale and multi-physics couplings in geo-environmental mechanics GDR CNRS 3176, 2008–2011) for having supported this work.

REFERENCES

1. Darve F, Servant G, Laouafa F, Khoa HDV. Failure in geomaterials, continuous and discrete analyses. *Computer Methods in Applied Mechanics and Engineering* 2004; **193**:3057–3085.
2. Nicot F, Darve F, Khoa HDV. Bifurcation and second-order work in geomaterials. *International Journal for Numerical and Analytical Methods in Geomechanics* 2007a; **31**:1007–1032.
3. Daouadji A, Darve F, Al Gali H, Hicher PY, Laouafa F, Lignon S, Nicot F, Nova R, Pinheiro M, Prunier F, Sibille L, Wan R. Diffuse failure in geomaterials, experiments, theory and modelling. *International Journal for Numerical and Analytical Methods in Geomechanics* 2011; **35**(16):1731–1773.
4. Lerbet J, Aldowaji M, Challamel N, Nicot F, Prunier F, Darve F. p-positive definite matrices and stability of non-conservative systems. *Zeitschrift für Angewandte Mathematik und Mechanik (ZAMM)* 2012; **92**(5):409–422.
5. Nicot F, Challamel N, Lerbet J, Prunier F, Darve F. Some insights into structure instability and the second order work criterion. *International Journal of Solids and Structures* 2012a; **49**(1):132–142.
6. Nicot F, Darve F. The *H*-microdirectional model: accounting for a mesoscopic scale. *Mechanics of Materials* 2011; **43**:918–929.
7. Šmilauer V, Catalano E, Chareyre B, Dorofeenko S, Duriez J, Gladky A, Kozicki J, Modenese C, Scholtès L, Sibille L, Stránský J, Thoeni K. Yade reference documentation. Yade Documentation (V. Šmilauer, ed.), The Yade Project, 1st ed. 2010. (Available from: http://yade-dem.org/doc/)
8. Nicot F, Darve F. A micro-mechanical investigation of bifurcation in granular materials. *International Journal of Solids and Structures* 2007; **44**:6630–6652.
9. Sibille L, Nicot F, Donze FV, Darve F. Material instabilities in granular assemblies from fundamentally different models. *International Journal for Numerical and Analytical Methods in Geomechanics* 2007; **31**(3):457–482.
10. Hill R. A general theory of uniqueness and stability in elastic–plastic solids. *Journal of the Mechanics and Physics of Solids* 1958; **6**:236–249.
11. Nicot F, Hadda N, Bourrier F, Sibille L, Wan R, Darve F. Inertia effects as a possible missing link between micro and macro second-order work in granular media. *International Journal of Solids and Structures* 2012b; **49**(10):1252–1258.
12. Love AEH. *A Treatise of Mathematical Theory of Elasticity*. Cambridge University Press: Cambridge, 1927.
13. Weber J. Recherches concernant les contraintes intergranulaires dans les milieux pulvérulents. Bulletin de Liaison des Ponts-et-Chaussées, n° 20, 1966; 1–20.
14. Christoffersen J, Mehrabadi MM, Nemat-Nasser S. A micro-mechanical description of granular material behavior. *Journal of Applied Mechanics* 1981; **48**:339–344.
15. Mehrabadi MM, Oda M, Nemat-Nasser S. On statistical description of stress and fabric in granular materials. *International Journal for Numerical and Analytical Methods in Geomechanics* 1982; **6**:95–108.
16. Bardet JB, Vardoulakis I. The asymmetry of stress in granular media. *International Journal of Solids and Structures* 2001; **38**:353–367.
17. Nicot F, Darve F. A multiscale approach to granular materials. *Mechanics of Materials* 2005; **37**(9):980–1006.
18. Nicot F, Darve F. Micro-mechanical investigation of material instability in granular assemblies. *International Journal of Solids and Structures* 2006; **43**:3569–3595.
19. Cambou B, Chaze M, Dedecker F. Change of scale in granular materials. *European Journal of Mechanics – A/Solids* Elsevier Ed. 2000; **19**:999–1014.
20. Bagi K. Analysis of microstructural strain tensors for granular assemblies. *International Journal of Solids and Structures* 2006; **43**:3166–3184.
21. Agnolin I, Jenkins JT, La Ragione L. A continuum theory for a random array of identical elastic frictional disks. *Mechanics of Materials* 2006; **38**(8–10):687–701.
22. Agnolin I, Kruyt NP. On the elastic moduli of two-dimensional assemblies of disks, relevance and modeling of fluctuations in particle displacements and rotations. *Computers and Mathematics with Applications* 2008; **55**:245–256.
23. Kuhn MR, Bagi K. Contact rolling and deformation in granular media. *International Journal of Solids and Structures* 2004; **41**:5793–5820.
24. Oda M, Konishi J, Nemat-Nasser S. Experimental micromechanical evaluation of strength of granular materials, effects of particle rolling. *Mechanics of Materials* 1982; **1**(4):269–283.

25. Oda M, Iwashita K, Kakiuchi T. Importance of particle rotation in the mechanics of granular materials. In *Powders and Grains 97, Balkema*, Behringer RP, Jenkins JT (eds). Publ: Rotterdam, Netherlands, 1997; 207–210.
26. Drescher A. An experimental investigation of flow rules for granular materials using optically sensitive glass particles. *Geotechnique* 1976; **26**:591–601.
27. Oda M, Konishi J. Microscopic deformation mechanism of granular material in simple shear. *Soils and Foundations* 1974; **14**(n 4):15–32.
28. Calvetti F, Combe G, Lanier J. Experimental micro-mechanical analysis of a 2D granular material, relation between structure evolution and loading path. *Mechanics of Cohesive-frictional Materials* 1997; **2**:121–163.
29. Gudehus G. A comparison of some constitutive laws for soils under radially symmetric loading and unloading. In 3rd Int. Conf. Numerical Methods in Geomechanics, Aachen, Wittke Ed., Balkema Publisher, 1979; **4**:1309–1324.
30. Laouafa F, Darve F. Modelling of slope failure by a material instability mechanism. *Computers and Geotechnics* 2002; **29**(4):301–325.
31. Chang C, Hicher PY, Daouadji A. Investigating instability in granular materials by means of a microstructural model. *European Journal of Environmental and Civil Engineering* 2009; **13**(2):167–186.
32. Wan RG, Pinheiro M, Guo PJ. Elastoplastic modelling of diffuse instability response of geomaterials. *International Journal for Numerical and Analytical Methods in Geomechanics* 2011; **35**(2):140–160.
33. Nicot F, Sibille L, Donzé F, Darve F. From microscopic to macroscopic second-order works in granular assemblies. *Mechanics of Materials* 2007b; **39**(7):664–684.
34. Sibille L, Donzé F, Nicot F, Chareyre B, Darve F. Bifurcation detection and catastrophic failure. *Acta Geotecnica* 2008; **3**(1):14–24.
35. Sibille L, Nicot F, Donzé F, Darve F. Analysis of failure occurrence from direct simulations. *European Journal of Environmental and Civil Engineering* 2009; **13**(2):187–202.
36. Cundall PA, Strack ODL. A discrete numerical model for granular assemblies. *Geotechnique* 1979; **29**:47–65.